Ultrasound-mediated extracellular matrix-preserving detachment suppresses extrinsic aging of mesenchymal stromal cells

Fumiko Tomatsu[†1], Jun Homma[†2], Shunsuke Yamagata[3], Hideharu Shimozawa[1], Shinsuke Mochizuki[1], Atsushi Nakamoto[1], Yoshikatsu Akiyama[2], Tatsuya Shimizu[2] & Chikahiro Imashiro*[3,2]

[†]These authors contributed equally to this work.

*Corresponding author

Chikahiro Imashiro

imashiro@pe.t.u-tokyo.ac.jp

1. Medical Business Operations, Canon Inc., 3-30-2 Shimomaruko, Ota-ku, Tokyo 146-8501, Japan.
2. Institute of Advanced Biomedical Engineering and Science, Tokyo Women's Medical University (TWIns), 8-1 Kawada-cho, Shinjuku-ku, Tokyo 162-8666, Japan.
3. Graduate School of Engineering, The University of Tokyo, 7-3-1 Hongo, Bunkyo-ku, Tokyo 113-8654, Japan.

Supplementary Note 1 | Characterization of the p53-immunoreactive band.

The polyclonal anti-p53 antibody used in this study detected an immunoreactive band migrating slightly below the apparent molecular weight of full-length p53 (~53 kDa). To examine the molecular identity of this band, we further probed the same samples with the N-terminal–specific monoclonal antibody DO-1, which selectively recognizes the N-terminal transactivation domain of full-length p53. DO-1 did not detect the corresponding band (Supplementary Fig. 1e). This antibody-dependent detection pattern is most parsimoniously explained by the presence of an N-terminally truncated p53 species, such as Δ40p53, which lacks the DO-1 epitope and migrates at a lower apparent molecular weight than full-length p53[1]. Importantly, Δ40p53 retains transcriptional activity toward a subset of p53 target genes and promotes cellular senescence in multiple cellular contexts[2]. Densitometric quantification across independent experiments (N = 3) is shown in Supplementary Fig. 1d. Individual data points are presented; statistical testing was not performed because of the limited sample size. The observed trend, passage-dependent upregulation under trypsinization and attenuation under ultrasound-mediated passaging, is consistent with the senescence-associated indicators presented in the main text. Although alternative interpretations such as partial proteolytic processing during sample preparation cannot be entirely excluded, the antibody specificity pattern, together with the biological context of long-term serial passaging, supports the interpretation that this band originates from a member of the p53 protein family.

Reference

1. Bourdon, J.-C. et al. p53 isoforms can regulate p53 transcriptional activity. *Genes Dev.* **19**, 2122–2137 (2005).
2. Ota, A. *et al.* Δ40p53α suppresses tumor cell proliferation and induces cellular senescence in hepatocellular carcinoma cells. *J. Cell Sci.* **130**, 614–625 (2017).

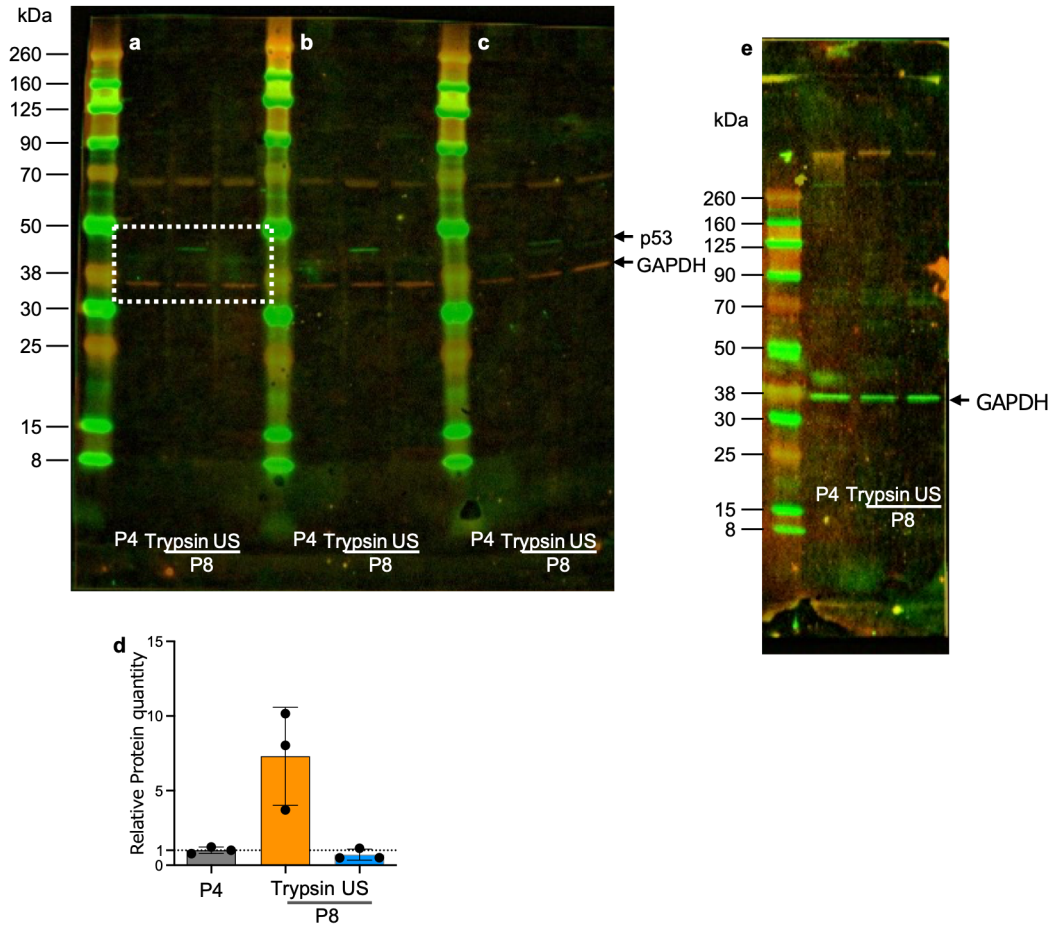

Supplementary Fig. 1 | Uncropped western blot images and densitometric analysis of p53-reactive bands. (a–c) Uncropped western blot images obtained using anti-p53 antibodies, including the blots corresponding to the data presented in Fig. 5c as well as additional independent experiments. All available blots are shown to ensure transparency.

(d) Densitometric quantification of the p53-reactive band detected across independent experiments (N = 3). Individual data points are shown. No statistical analysis was performed because of the ambiguous molecular identity of the detected band.

(e) Western blot analysis of the same samples probed with the N-terminal-specific monoclonal antibody DO-1, showing the absence of the corresponding p53-reactive band.

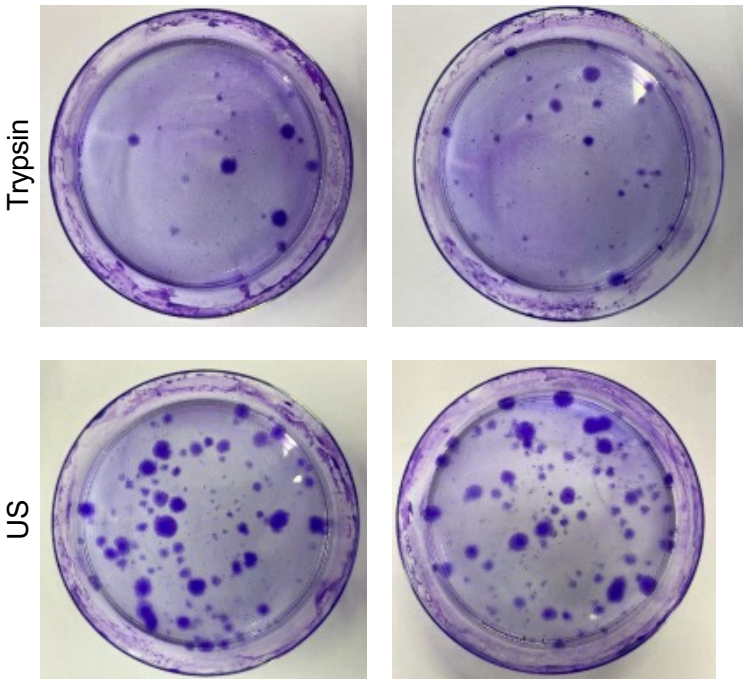

Supplementary Fig. 2 | Additional colony formation assay results from independent experiments.

Representative images of colony formation assays from additional independent experiments not included in the main figures. These data are provided to demonstrate the reproducibility of the findings.

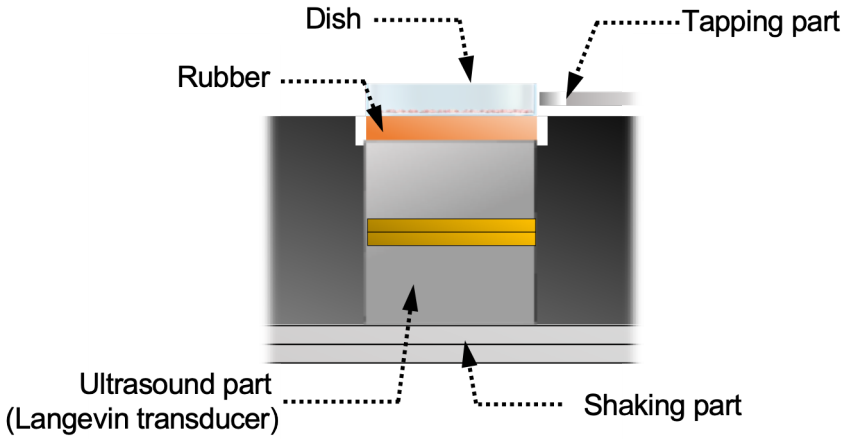

Supplementary Fig. 3 | Cross-sectional view of CEPUS.

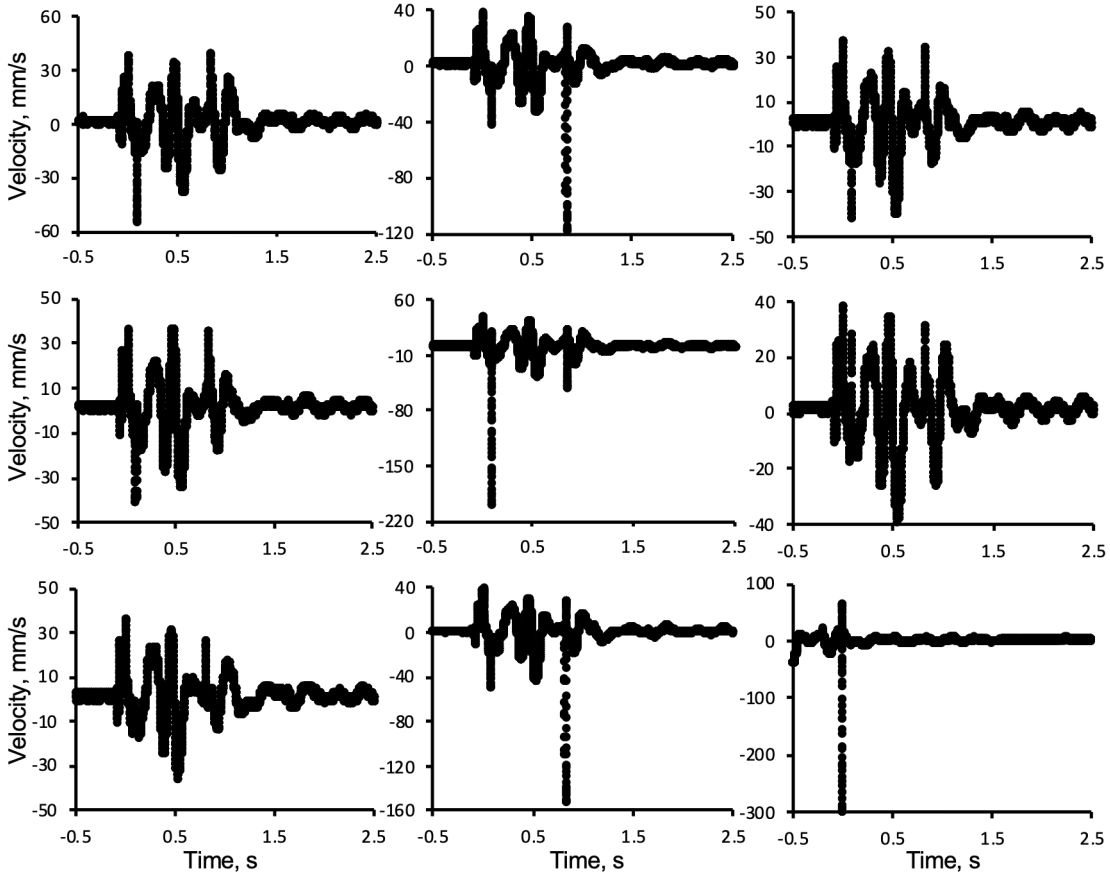

Supplementary Fig. 4 | Raw vibration signals used for FFT analysis.

Time-domain vibration velocity signals measured during mechanical tapping (N = 10). The dataset includes all measurements except for the representative signal shown in Fig. 2c. Each signal was analyzed individually using FFT, and the resulting spectra were subsequently averaged.

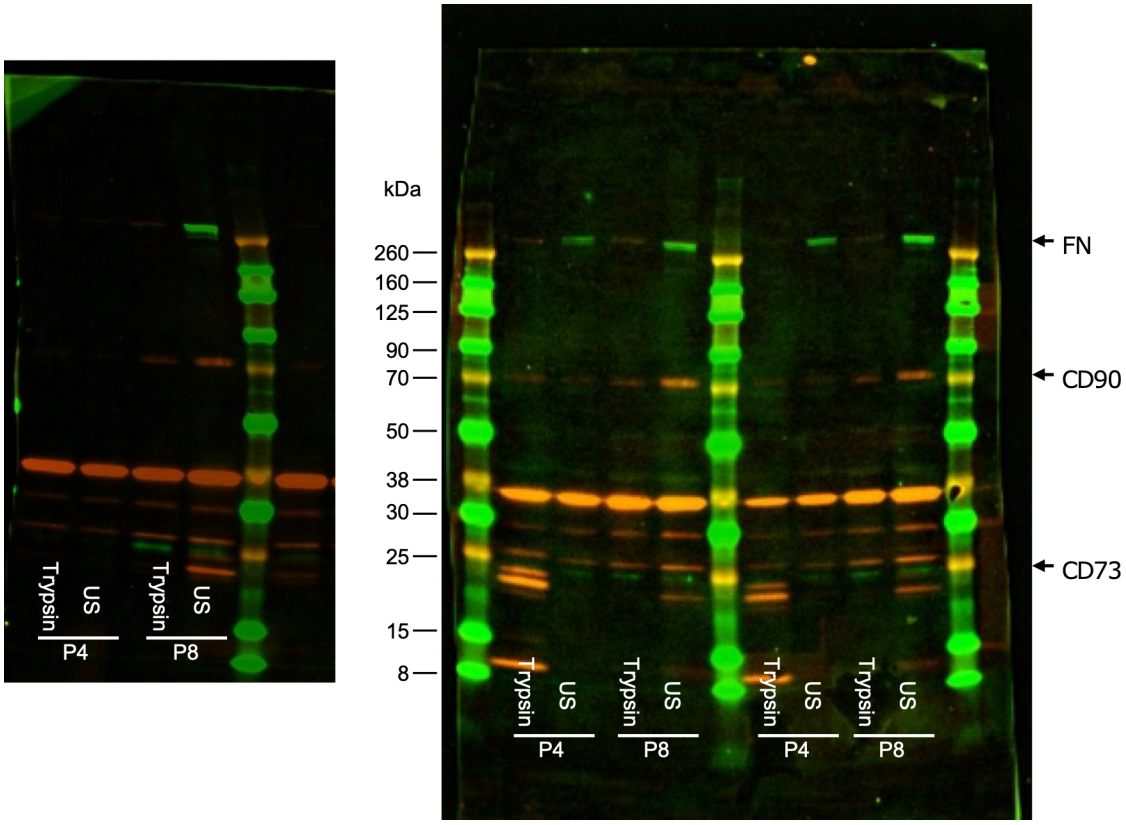

Supplementary Fig. 5 | Uncropped western blot images corresponding to Figs. 3e, f, and 6g–j).

Supplementary Table 1. Statistical analysis of cell area (Fig. 4c)

Effect / Comparison	Test	Statistic (df)	*P*-value
Method	Two-way ANOVA	F(1,8) = 10.7	0.0111
Passage	Two-way ANOVA	F(1,8) = 36.2	0.0003
Method × Passage	Two-way ANOVA	F(1,8) = 0.44	0.5237
Trypsin P5 vs Trypsin P8	Tukey's post hoc	—	0.0065
Trypsin P8 vs US P5	Tukey's post hoc	—	0.0008
US P5 vs US P8	Tukey's post hoc	—	0.0223
Other comparisons	Tukey's post hoc	—	>0.05

Supplementary Table 2. Statistical analysis of nuclear area (Fig. 4d)

Effect/Comparison	Test	Statistic (df)	*P*-value
Method	Two-way ANOVA	F (1,8) = 5.66	0.0445
Passage	Two-way ANOVA	F (1,8) = 0.28	0.6105
Method × Passage	Two-way ANOVA	F (1,8) = 7.63	0.0246
Trypsin P5 vs Trypsin P8	Tukey's post hoc	—	0.4402
Trypsin P5 vs US P5	Tukey's post hoc	—	0.9925
Trypsin P5 vs US P8	Tukey's post hoc	—	0.2448
Trypsin P8 vs US P5	Tukey's post hoc	—	0.5831
Trypsin P8 vs US P8	Tukey's post hoc	—	0.0273
US P5 vs US P8	Tukey's post hoc	—	0.1703

Supplementary Table 3. Statistical analysis of nuclear aspect ratio (Fig. 4e)

Effect/Comparison	Test	Statistic (df)	*P*-value
Method	Two-way ANOVA	F (1,8) = 7.38	0.0264
Passage	Two-way ANOVA	F (1,8) = 6.26	0.0367
Method × Passage	Two-way ANOVA	F (1,8) = 6.62	0.0329
Trypsin P5 vs Trypsin P8	Tukey's post hoc	—	0.0291
Trypsin P5 vs US P5	Tukey's post hoc	—	0.9996
Trypsin P5 vs US P8	Tukey's post hoc	—	0.9987
Trypsin P8 vs US P5	Tukey's post hoc	—	0.0253
Trypsin P8 vs US P8	Tukey's post hoc	—	0.0236
US P5 vs US P8	Tukey's post hoc	—	>0.9999

Supplementary Table 4. Statistical analysis of colony number (Fig. 6c)

Effect/Comparison	Test	Statistic (df)	*P*-value
US vs Trypsin	Welch's t test	t (2.905) = 5.936	0.0105